RSC Advances

This article can be cited before page numbers have been issued, to do this please use: Y. Liu, J. Chen and Y. ZHANG, *RSC Adv.*, 2015, DOI: 10.1039/C5RA02319J.

ROYAL SOCIETY OF CHEMISTRY

www.rsc.org/advances

Cite this: DOI: 10.1039/c0xx00000x

www.rsc.org/xxxxxx

COMMUNICATION

The effect of pore size or iron particle size on formation of light olefins in Fischer–Tropsch synthesis

Yi Liu,[a] Jian-Feng Chen[b] and Yi Zhang*[a,b]

Received (in XXX, XXX) Xth XXXXXXXXX 20XX, Accepted Xth XXXXXXXXX 20XX
DOI: 10.1039/b000000x

The surface modification of silica support was applied in solely comparing the effects of iron particle size or pore size on forming light olefins. Smaller iron or iron carbide particle is advantageous to form light olefins and O/P of C_2-C_4 is more sensitive to the pore size of catalysts.

Fischer–Tropsch synthesis has long been known as one of the key technologies for producing ultra-clean fuels from non-crude-oil feedstocks. Comparing to ruthenium or cobalt catalysts, iron-based catalysts are advantageous due to their high selectivity of olefins, low costs, and tolerance to high temperatures and moisture environments. [1] Previously, researchers showed that syngas can be converted to olefins via F-T synthesis, by using bulk or supported iron-based catalysts. [2-4]

For supported iron-based catalysts, several researchers have suggested that the texture properties of the support have a significant influence on the FTS activity and light olefins selectivity. [5-8] Generally, small pore size is advantageous to formation of small supported metal particles and promotes the dispersion of supported metal. [9-11] However, the small pore size of supports results in poor diffusion efficiency of reactants and products, which is a disadvantage to catalytic performance of catalysts. In contrast, the support with a larger pore size improves the reducibility, improves the diffusion of reactants and products, suppresses the re-adsorption of 1-olefins, and leads to high heavy hydrocarbon content in the products. [5, 7, 12] However, the increased chain-growth probability occurring on the larger pore catalyst might be attributed to the combined effects of larger metal particle size and larger pore size. It was found that both the dispersion of the supported metal and the pore size of the catalyst showed their close relationship with the propagation of the carbon chain.

Although a few studies were carried out on the influence of the iron particle size and the pore size of support on the FTS reaction activity and selectivity, controversy persists, because these observations were the results of complex interplay among many factors. These factors included not only the re-adsorption probability of α-olefins in the confined space and the diffusion situation, but also the effect of changes in the site density, such as the changes in loading, reducibility and the particle size of active metal. [1] Hence, it is difficult to evidence the effects of the support porosity on activity and selectivity, since the metal dispersion or the metal particle size also depends on the pore size distribution. More insights are expected to prepare catalysts with a fixed pore size with different particle size, or a fixed particle size of active metals with different pore sizes.

In the present work, in order to investigate the sole effect of pore size or iron particle size on formation of light olefins in Fischer–Tropsch synthesis (FTS), the various iron supported catalysts with pore size of 5 nm, 50 nm and 80 nm were prepared by surface modification of silica support by ethylene glycol to realize the similar iron particle size. The similar properties of iron active phase on different catalysts guaranteed solely comparing the effect of pore size on formation of light olefins. For sole comparing effects of particle size, the conventional impregnation method was applied to prepare the catalysts contained large iron particle size and the same pore size.

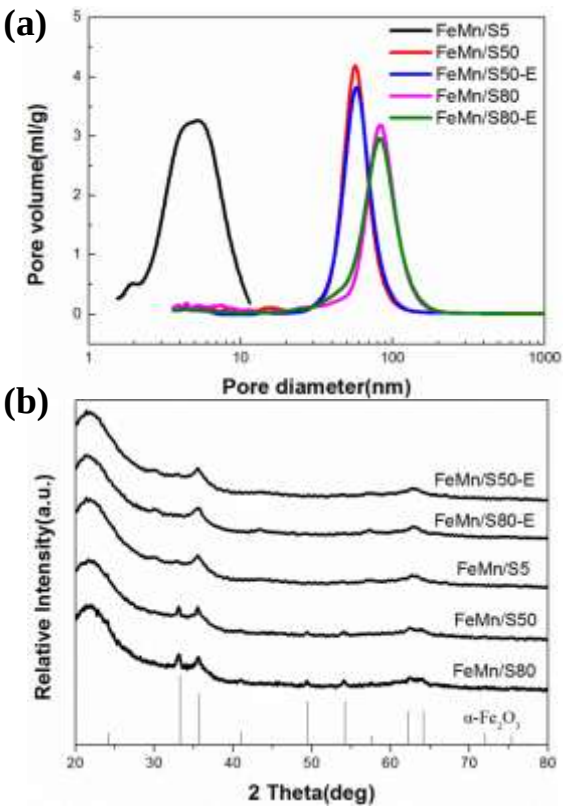

Fig. 1 (a) Pore size distribution of silica supported iron-based catalysts as prepared, (b) X-ray diffractograms of silica supported iron-based catalysts as prepared.

The textural properties of obtained catalysts were characterized

View Article Online
DOI: 10.1039/C5RA02319J

by N_2 physisorption and mercury intrusion porosimetry. As shown in Fig. 1a, the pore size distributions of all iron-based catalysts show monomodal pore size distributions, indicating there are not newly formed pores inside the original pores contributing to solely compare effects of pore size on light olefin formation. XRD was used to analyze the crystalline phases present in the catalysts after calcination. As show in Fig. 1b, no peaks assigned to manganese species were observed on these samples, due to very small loading of Mn. It is found that the particle size increase from 8.1 to 17.5 nm for samples with constant metal loading on increasing the pore size from 5 to 80 nm. For the ethylene glycol pretreated catalysts, the particle size of the FeMn/S80-E and FeMn/S50-E catalysts decreased significantly from original FeMn/S80 and FeMn/S50 catalysts and were very close to that of FeMn/S5, as shown in Table 1 and Fig. 1b. It is proved that the pretreatment of silica supports by ethylene glycol remarkably modified the properties of the silica surface and increased the isolated SiOH ratio on the silica surface, [13] resulting in lower crystalline size of supported iron oxide. On the other hand, it is considered that during the calcination step, the heat uniformly released from thermal decomposing of oxyl group derived from ethylene glycol was quickly absorbed by the precursor of catalyst to supply energy for decomposition of nitrates, which efficiently restrained the aggregation of the iron oxides, resulting in smaller particle size. [14]

Table 1 Various properties of silica supported iron-based catalysts.

Catalysts	Pore Size (nm)	Pore Volume (cm^3/g)	Specific Surface Area (m^2/g)	d(Fe_2O_3) (nm)[a]	d(Fe_2O_3) (nm)[b]	d(Fe_5C_2) (nm)[c]	Mn/Fe atomic ratio[d]	Fe reducibility (%)[e]
FeMn/S80	84.6	0.93	70.4	17.5	17.1	18.2	0.37	41.9
FeMn/S50	51.9	0.95	111.4	13.7	13.8	15.2	0.29	39.4
FeMn/S5	4.9	0.80	372.8	8.1	7.9	8.2	0.09	32.0
FeMn/S50-E	54.0	0.91	78.2	8.2	8.5	8.3	0.10	29.0
FeMn/S80-E	83.1	0.93	73.5	8.2	8.0	8.2	0.09	29.9

[a] Fe_2O_3 crystallite size as determined by X-ray diffraction. [b] Fe_2O_3 crystallite size as determined by TEM. [c] Fe_5C_2 crystallite size as determined by TEM after reduction. [d] Determined by XPS, the stoichiometric Mn/Fe atomic ratio of all catalysts is 0.05. [e] Calculated by H_2-TPR.

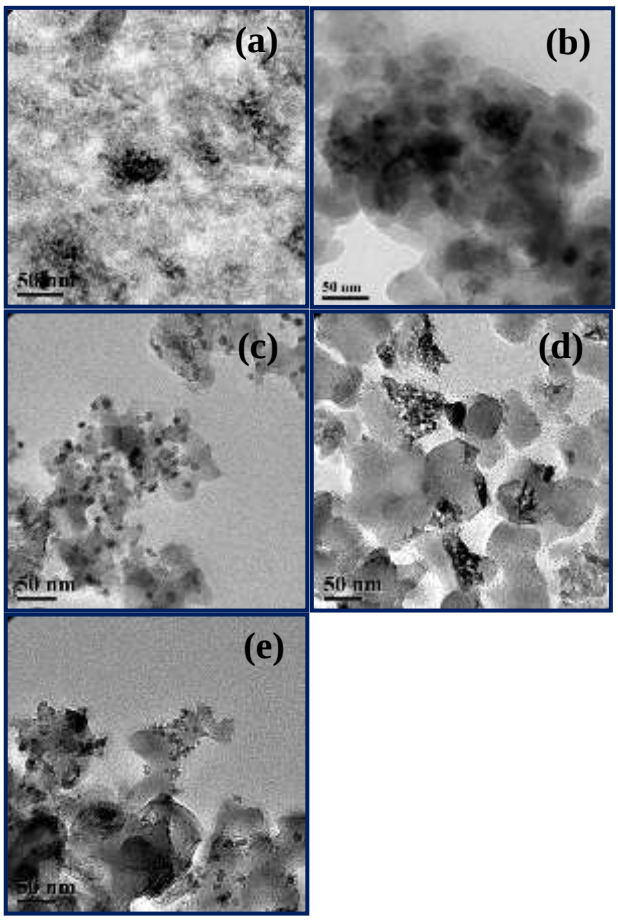

Fig. 2 TEM micrographs for silica supported iron-based catalysts on (a) FeMn/S5, (b) FeMn/S50, (c) FeMn/S50-E, (d) FeMn/S80 and (e) FeMn/S80-E as prepared.

Fig. 2 and Fig. S1 show the TEM images and the particle size distribution of various iron-based catalysts. The results are in agreement with the XRD analysis, indicating that the average iron particle size increases with increasing pore size. Meanwhile, for the catalysts pretreated by EG, significant differences in Fe_2O_3 particle size have been observed (Fig. 2c and e). The FeMn/S80-E and FeMn/S50-E catalysts exhibited homogeneous remarkable smaller particle size than that of FeMn/S80 and FeMn/S50, respectively. The TEM images of various reduced iron catalysts were compared in Fig. S2. As shown in Table 1, the size of iron carbide kept the same trend to the iron particle size of various catalysts.

The iron phase composition and dispersion of the fresh catalysts were also determined by Mössbauer spectroscopy. As shown in Fig. 3, the MES spectra of the fresh FeMn/S50 catalyst include a sextet and a doublet, whereas the MES spectra of the FeMn/S50-E and FeMn/S5 catalysts include only a doublet. According to the MES parameters listed in Table S1, the sextet is assigned to the magnetic α-Fe_2O_3 with crystallites size larger than 13.5 nm. [15] The doublet is typical for the superparamagnetic (spm) Fe^{3+} ions on the non-cubic sites with the crystallite diameters smaller than 13.5 nm. [16,17] The FeMn/S50 consists of 62.8% ferromagnetic α-Fe_2O_3 and 37.2% Fe^{3+} (spm) and the FeMn/S50-E and FeMn/S5 are composed of 100% Fe^{3+} (spm). This result suggests that the average Fe_2O_3 particle size of FeMn/S50 were larger than those of FeMn/S50-E and FeMn/S5. In addition, for the FeMn/S50-E and FeMn/S5 catalysts, the ratio of the atoms located on the ''surface'' of the crystallites to the atoms located in the ''bulk'' of the crystallites was similar. This result indicates that the average iron oxide particle sizes were almost identical for FeMn/S50-E and FeMn/S5, [18, 19] and it is well consistent with the results of TEM and XRD characterization. Based on these findings, the similar particle structure of catalysts with different pore size contributes to solely investigate the pore size effects, and the same pore size of catalysts with different iron particle

View Article Online
DOI: 10.1039/C5RA02319J

size is advantageous to solely comparing the particle size effects on selectivity of light olefins.

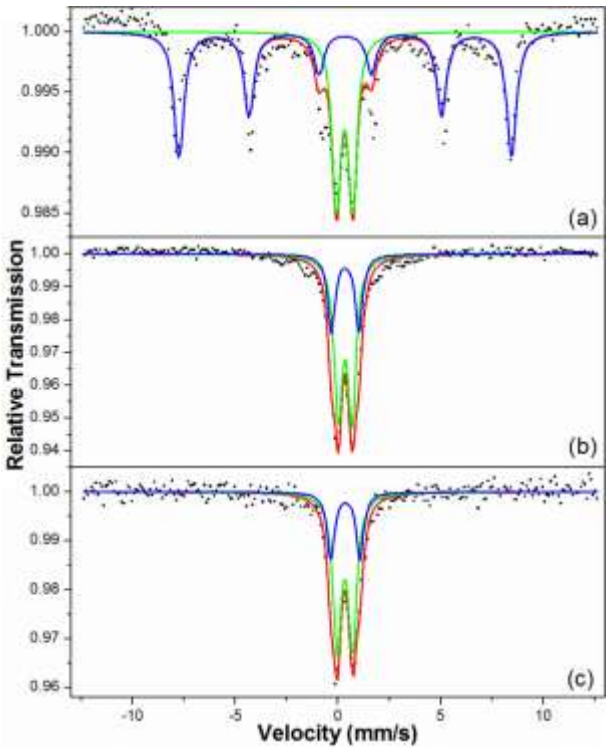

Fig. 3 Mössbauer spectra of the fresh iron-based catalysts: (a) FeMn/S50; (b) FeMn/S50-E; (c) FeMn/S5.

In order to identify the chemical properties of iron particle, the XPS analysis was carried out to determine the surface chemical composition and electronic structures of iron particle with different size. The Fe 2p spectrum (Fig. 4) displays the main peaks of Fe $2p_{3/2}$ at the binding energies between 710.4 and 711.3 eV, together with a very weak satellite structure between the spin–orbit doublet. This result indicates that Fe species are characteristic of trivalence in α-Fe_2O_3. [20, 21] Concerning the binding energy of Fe2p of various catalysts, it slightly decreased with increased iron particle size. Meanwhile, the catalysts with the almost same particle size showed the same binding energy. It is considered that the large iron particle of FeMn/S80 and FeMn/S50 catalyst increased electron density of surface iron atom, leading to lower binding energy. On the other hand, it has been reported that manganese oxide could act as surface basicity as alkali metal does, [22, 23] namely, manganese oxide might act as a strong electron donor. Therefore, the Fe/Mn ratio of the iron particle surface was determined by XPS also. As compared in Table 1, the Fe/Mn ratio was increased with increasing iron particle size, and FeMn/S80-E, FeMn/S50-E and FeMn/S5 catalysts exhibited the almost same Fe/Mn ratio, indicating that Mn enriched on the surface of larger iron particle and would exhibited different promotional effects for larger iron particles, comparing to smaller one. Meanwhile, for the FeMn/S80-E, FeMn/S50-E and FeMn/S5 catalysts, the similar Fe/Mn ratio indicated the promotional effects of added Mn on EG pretreated catalysts were similar to the non-pretreated one, contributing to solely comparing the effects of pore size on light olefin formation.

The reduction behavior of the silica supported iron-based catalysts was measured by temperature programmed reduction (TPR). The H_2-TPR profiles of the catalysts are presented in Fig. 5. It is clearly shown that the reduction process of the catalysts all occurs in two main stages. The first stage at low temperature (250-400℃) is attributed to the transformations of $Fe_2O_3 \rightarrow Fe_3O_4$ and part of $Fe_3O_4 \rightarrow FeO$, whereas the second stage at higher temperature (400-550℃) correspond to the reduction of the remainder of Fe_3O_4 and FeO, and the peak above 600℃ should be ascribed to the reduction of wustite (FeO) or Fe_2SiO_4, which strongly interacted with SiO_2. [24, 25] In addition, it is found that the temperature of the reduction peak shifts to high temperature with a decrease of Fe_2O_3 particle size, due to strong interaction with silica support of small iron particle. On the other hand, the catalysts with similar iron particle size, such as FeMn/S5, FeMn/S50-E and FeMn/S80-E, exhibited very similar reduction profile, contributing to the similar properties of active phase during FTS reaction. As compared in Table 1, the reducibility of FeMn/S50 and FeMn/S80 was higher than that of catalysts with smaller iron particles. In addition, based on the XPS results (Table 1), it was observed that the Mn/Fe atomic ratio on the catalyst surface increased from 0.09 of FeMn/S5 to 0.37 of FeMn/S80 when the Fe_2O_3 particle size increased from 8.1 to 17.5 nm. It is considered that the different reducibility and Mn/Fe atomic ratio of the catalysts with large iron particle could influence the reaction performance during FTS reaction.

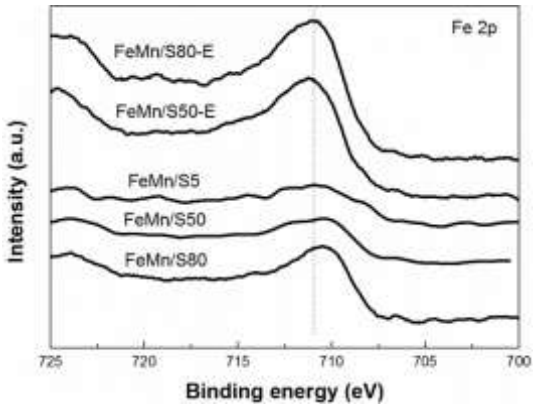

Fig. 4 XPS spectra of Fe 2p on silica supported iron-based FTS catalysts as prepared.

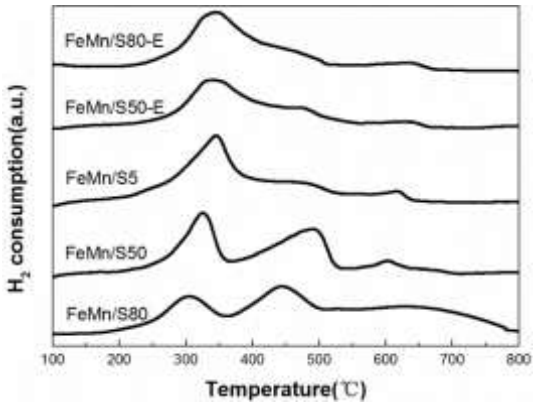

Fig. 5 H_2-TPR profiles of silica supported iron-based catalysts.

To investigate the sole effects of pore size and particle size on the catalytic performance, the obtained catalysts were applied to fixed-bed FTS reaction. As compared in Fig. S3, the FeMn/S80-E

View Article Online
DOI: 10.1039/C5RA02319J

catalyst realized the highest CO conversion in all catalysts. Meanwhile, both FeMn/S50-E and FeMn/S80-E catalysts exhibited excellent stability during 30 h reaction. As reported in our previous literature, [7] the pore size of catalyst could influence the catalytic activity because of the differences in the diffusion of both reactants and products. On the other hand, smaller iron carbide clusters of fine dispersed iron catalysts are less prone to deactivation. [26] Therefore, for FeMn/S80-E catalyst, the largest pore size and very small iron carbide particle size is advantageous to realize the high activity and good stability. Because FeMn/S80-E and FeMn/S80 catalysts contained the same pore size, it is considered that smaller iron particle size is advantageous to obtain high activity and stability for iron based FTS catalyst.

Although a few studies were carried out on the influence of the iron particle size and the pore size of support on the FTS reaction selectivity, controversy persists, because these observations are the result of complex interplay among many factors. In this study, the sole effect of pore size or iron particle size was investigated for forming light olefins in Fischer–Tropsch synthesis (FTS).

Table 2 Catalytic activity and product selectivity of silica supported iron-based catalysts. [a]

Catalysts	CO conv. (%)	CO_2 (%CO conv.)	Hydrocarbon selectivity (c-mol %, CO_2-free)				C_2-C_4 Olefin/P araffin
			CH_4	$C^{=}_{2-4}$	C_{2-4}	C_{5+}	
FeMn/S80	40.0	33.9	8.5	48.2	10.7	32.6	4.50
FeMn/S50	44.0	34.1	11.7	43.5	15.5	29.3	2.81
FeMn/S5	21.9	24.3	24.2	30.2	27.2	18.4	1.11
FeMn/S50-E	48.3	32.9	14.8	51.2	14.2	19.8	3.61
FeMn/S80-E	50.5	33.4	13.3	54.6	11.7	20.4	4.67

[a] Reaction condition: 573 K, 1.0 MPa, H_2/CO=1, W/F(CO+H_2+Ar) =5 g-cat. h mol^{-1}, Weight of catalyst =0.5 g.

The selectivities of light olefins and methane as function of pore size were compared in Fig. 6. For the catalysts obtained from conventional preparation method, as shown in Fig. 6a, the selectivity of light olefins increased from 30.2% for FeMn/S5 to 48.2% for FeMn/S80, and methane selectivity significantly decreased from 24.2% to 8.5% for FeMn/S5 and FeMn/S80, respectively. The tendency of olefin to paraffin ratio (O/P) was also increased from 1.11 to 4.50 for FeMn/S5 and FeMn/S80 as compared in Table 2. However, the FeMn/S80 catalyst formed much more liquid products (C_{5+}) than FeMn/S5 catalysts, as the selectivity of liquid products (C_{5+}) was 32.6% and 18.4%, respectively. It is well know that the support with a larger pore size favors the diffusion of reactants and products, suppresses the re-adsorption of 1-olefins, and leads to high heavy hydrocarbon content in the product. [5] Therefore, the catalysts with larger pore size, such as FeMn/S50 and FeMn/S80, formed much more liquid hydrocarbon and less methane. However, as the improved diffusion efficiency in larger pore, the second reactions of formed light olefins were suppressed, leading to the increased light olefin selectivity with the increased pore size.

It should be point out that the FeMn/S80 catalyst contained both large pore size and large iron particle size, and the reaction performance of this catalyst should be the synergetic effects of large pore size and particle size. It is considered that the lowest methane selectivity contributes the highest light olefin and liquid hydrocarbon selectivity for FeMn/S80 catalyst in catalysts prepared by conventional impregnation method.

As shown in Fig. 6 b and Table 2, when the iron particle size was similar for different catalysts, the selectivity of light olefin significantly increased with the increased pore size of catalysts, from 30.2% for FeMn/S5 to 54.6% for FeMn/S80-E. And the ratio of olefin to paraffin (O/P) in C_2-C_4 hydrocarbon also increased with increasing pore size. Furthermore, the formation of CH_4 was suppressed with increasing pore size, which decreased from 24.2% to 13.3% for FeMn/S5 and FeMn/S80-E, respectively. However, the liquid hydrocarbons (C_{5+}) selectivity was similar for different catalysts as around 19%, as shown in Table 2.

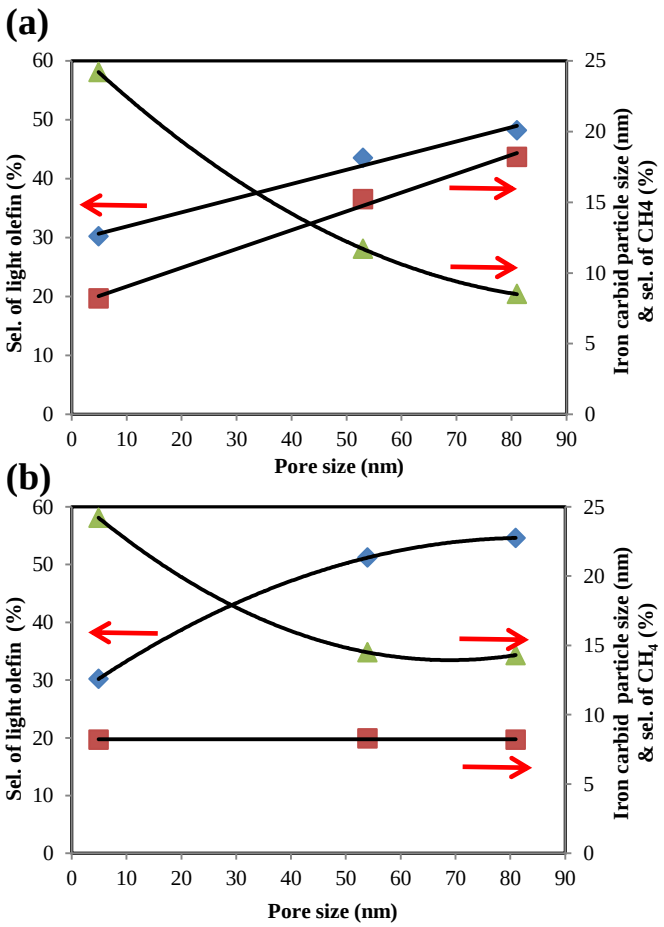

Fig. 6 Product selectivity as a function of pore size: (a) nonpretreated catalysts; (b) EG-pretreated catalysts; light olefin (◆); methane (▲); iron carbide particle size (■).

For FeMn/S50-E and FeMn/S80-E catalysts, however, the methane selectivity was remarkably enhanced than that of FeMn/S50 and FeMn/S80 catalysts, when the iron carbide particle size significantly decreased. Meanwhile, the methane selectivity of the FeMn/S50-E and FeMn/S80-E catalysts was very similar as 14.8% and 13.3%, respectively. On contrast, the methane selectivity of FeMn/S50 catalyst was higher than that of FeMn/S80 catalyst. The selectivity of liquid hydrocarbon also exhibited similar tendency. As compared in Fig. 6 and Table 2, the FeMn/S50-E and FeMn/S80-E catalysts contained the almost same iron carbide particle size (Fig. 6 b), and the FeMn/S50 catalyst exhibited smaller iron carbide particle size than

View Article Online
DOI: 10.1039/C5RA02319J

FeMn/S80. On the other hand, the FeMn/S80-E and FeMn/S80 catalysts had much larger pore size than the FeMn/S50-E and FeMn/S50 catalysts. Base on these results, it is considered that the selectivity of methane and liquid hydrocarbons (C_{5+}) strongly depended on iron particle size or iron carbide particle size, namely, smaller iron particle or iron carbide particle was much beneficial to forming light hydrocarbons including methane.

Concerning the selectivity of light olefins, the FeMn/S5, FeMn/S50-E and FeMn/S80-E catalysts exhibited the increased light olefins selectivity with the increased pore size, as illustrated in Fig. 6 b. Because these catalysts contained the same iron particle size, and it is proved that those iron particles had similar bulk and surface properties as proved by XRD, TEM, XPS, TPR and Mössbauer spectroscopy. It is believed that the large pore size could contribute to the formation of light olefins via suppressing the second reaction of formed olefins including hydrogenation, isomerization and chain-growth reaction. [27] On the other hand, as illustrated by Fig. 7, the olefin to paraffin ratio (O/P) of C_2-C_4 hydrocarbons significantly increased from small pore catalyst to large pore catalyst regardless of iron carbide particle size, indicating the O/P of C_2-C_4 hydrocarbons was more sensitive to pore size of catalysts.

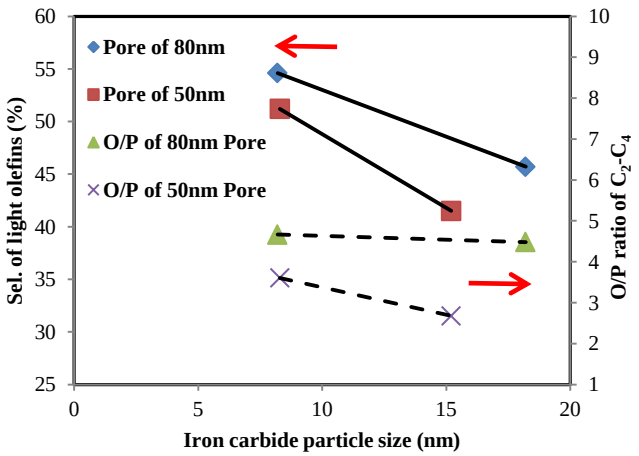

Fig. 7 Light olefin selectivity and O/P ratio of C_2-C_4 as a function of iron carbide particle size.

For the catalysts with the same pore size but different iron carbide particle size, the one with smaller iron particle size realized much higher selectivity of light olefins. It is well known that manganese can restrain the hydrogenation ability, suppress the formation of methane, [28] and enhance the selectivity of light olefins. [29, 30] For large iron particles in this study, Mn enriched on the surface of iron particle as proved by XPS, which would enhance the promotional effects of Mn on forming light olefins. [30] However, as compared in Fig. 7, the FeMn/S50 and FeMn/S80 catalysts exhibited much lower light olefins selectivity than FeMn/S50-E and FeMn/S80-E, those contained much smaller iron carbide particles. On the other hand, the light olefins selectivity of FeMn/S80-E catalyst only slightly increased from 51.2% of FeMn/S50-E catalyst to 54.6%, even though FeMn/S80-E catalyst had larger pore size than FeMn/S50-E catalyst. Therefore, it is considered that the formation of light olefins on silica supported FeMn was more sensitive to iron or iron carbide particle size, namely, smaller iron or iron carbide particles was advantageous to form more light olefins.

Conclusions

The sole effect of iron particle size or pore size was investigated on formation of light olefins in Fischer–Tropsch synthesis (FTS). The obtained catalysts with the same pore size and similar properties of iron active phase guaranteed solely comparing the effect of iron particle size on formation of light olefins. The smaller iron particle is much beneficial to forming light hydrocarbons including methane. Furthermore, smaller iron particle is advantageous to form more light olefins. Meanwhile, the olefin to paraffin ration (O/P) of C_2-C_4 hydrocarbons is more sensitive to pore size of catalysts due to suppressing the second reaction of formed olefins.

Acknowledgment

This work was supported by National Natural Science Foundation of China (Nos. 91334206, 51174259), Ministry of Education (NCET-13-0653), National "863" program of China (No. 2012AA051001 and 2013AA031702).

Notes and references

[a] *State Key Laboratory of Organic–Inorganic Composites, Department of Chemical Engineering, Beijing University of Chemical Technology, Beijing 100029, China. Fax: 86-10-64423474; Tel: 86-10-64447274; E-mail: yizhang@mail.buct.edu.cn*

[b] *Research Centre of the Ministry of Education for High Gravity Engineering and Technology, Beijing University of Chemical Technology, Beijing 100029, China. E-mail: chenjf@mail.buct.edu.cn*

† Electronic Supplementary Information (ESI) available: Experimental details, Mössbauer parameters of the fresh iron-based catalysts, TEM micrographs for the catalysts after reduction and CO conversion as a function of time on stream. See DOI: 10.1039/b000000x/

1 Q. H. Zhang, J. C. Kang and Y. Wang, *ChemCatChem*. 2010, **2**, 1030.
2 C. Wang, L. Xu and Q. Wang, *J. Nat. Gas. Chem*. 2003, **12**, 10.
3 B. Büssemeier, C. D. Frohning, G. Horn and W. Kluy, US Patent 4564642, 1986.
4 L. Bruce, G. Hope and T. W. Turney, *React. Kinet. Catal. Lett.* 1982, **20**, 175.
5 B. Xu, Y. Fan, Y. Zhang and N. Tsubaki, *AIChE J.* 2005, **51**, 2068.
6 Y. Liu, K. Fang, J. Chen and Y. Sun, *Green Chem.* 2007, **9**, 611.
7 L. Fan, K. Yokota and K. Fujimoto, *AIChE J.* 1992, **38**, 1639.
8 X. Chen, D. Deng, X. Pan, Y. Hu, X. Bao, *Chem. Commun.* 2015, **51**, 217.
9 J.P. Hong, P.A. Chernavskii, A.Y. Khodakov, W. Chu, *Catal. Today*. 2009, **140**, 135.
10 N. Yao, H. Ma, Y. Shao, C. Yuan, D. Lv, X. Li, *J. Mater. Chem.* 2011, **21**, 17403.
11 Y. Zhang, Y. Yoneyama and N. Tsubaki, *Chem. Commun.* 2002, **11**, 1216.
12 N. Tsubaki, Y. Zhang, S. Sun, H. Mori, Y. Yoneyama, X. Li and K. Fujimoto, *Catal. Commun.* 2001, **2**, 311.
13 J. F. Chen, Y. R. Zhang, L. Tan and Y. Zhang, *Ind. Eng. Chem. Res.* 2011, **50**, 4212.
14 X. Lv, J. F. Chen, Y. Tan and Y. Zhang, *Catal. Commun.* 2012, **20**, 6.
15 H. M. T. Galvis, J. H. Bitter, C. B. Khare, M. Ruitenbeek, A. I. Dugulan and K. P. de Jong, *Science*. 2012, **335**, 835.
16 J. W. Niemantsverdriet and A. M. Van der Kraan, *J. Phys. Chem.* 1985, **89**, 67.
17 J. Yang, Y. Sun, Y. Tang, Y. Liu, H. Wang, L. Tian, H. Wang, Z. Zhang, H. Xiang and Y. W. Li, *J. Mol. Catal. A* 2006, **245**, 26.
18 H. Dlamini, T. Motjope, G. Joorst, G. Stege and M. Mdleleni, *Catal. Lett.* 2002, **78**, 201.

View Article Online
DOI: 10.1039/C5RA02319J

19 E. S. Lox, G. B. Marin, R. de Grave and P. Bussiere, *Appl. Catal.* 1988, **40**, 197.
20 J. Cao, Y. Wang, X. Yu, S. Wang, S. Wu and Z. Yuan, *Appl. Catal. B* 2008, **79**, 26.
21 T. Yamashita and P. Hayes, *Appl. Surf. Sci.* 2008, **254**, 2441.
22 M. E. Dry and G. J. Oosthuizen, *J. Catal*. 1968, **11**, 18.
23 K. B. Jensen and F. E. Massoth, *J. Catal*. 1985, **92**, 98.
24 M. Qing, Y. Yang, B. Wu, J. Xu, C. Zhang, P. Gao and Y. W. Li, *J. Catal*. 2011, **279**, 111.
25 J.P. Hong, W. Chu, P.A. Chernavskii, A.Y. Khodakov, *J. Catal*. 2010, **273**, 9.
26 A. Campos, N. Lohitharn, A. Roy, E. Lotero, J. G. Goodwin Jr. and J. J. Spivey, *Appl. Catal. A* 2010, **375**, 12.
27 H. Schulz, *Catal. Today*. 2014, **228**, 113.
28 Z. Tao, Y. Yang, C. Zhang, T. Li, M. Ding, H. Xiang and Y. W. Li, *J. Nat. Gas. Chem.* 2007, **16**, 278.
29 J. Barrault and C. Renard, *Appl. Catal.* 1985, **14**, 133.
30 K. M. Kreitman, M. Baerns and J. B. Butt, *J. Catal*. 1987, **105**, 319.